1990ApJ...363..422K

THE ASTROPHYSICAL JOURNAL, 363:422–434, 1990 November 10
© 1990. The American Astronomical Society. All rights reserved. Printed in U.S.A.

VACUUM ULTRAVIOLET IMAGERY OF THE VIRGO CLUSTER REGION. II. TOTAL FAR-ULTRAVIOLET FLUX OF GALAXIES

K. KODAIRA AND T. WATANABE
National Astronomical Observatory, Japan

AND

T. ONAKA AND W. TANAKA
Department of Astronomy, University of Tokyo
Received 1990 March 15; accepted 1990 May 3

ABSTRACT

The total flux in the far-ultraviolet region around 150 nm was measured for more than 40 galaxies in the central region of the Virgo Cluster, using two imaging telescopes on board a sounding rocket. The observed far-ultraviolet flux shows positive correlations with the H I 21 cm flux and the far-infrared flux for spiral galaxies, and with the X-ray flux and the radio continuum flux for elliptical galaxies. The former correlations of spiral galaxies are interpreted in terms of star formation activity, which indicates substantial depletion in the Virgo galaxies in accordance with the H I stripping. The latter correlations of elliptical galaxies indicate possible far-ultraviolet sources of young population, in addition to evolved hot stars. Far-ultraviolet fluxes from two dwarf elliptical galaxies were obtained tentatively, indicating star formation activity in elliptical galaxies. A high-resolution UV imagery by *HST* would be effective to distinguish the young population and the old population in elliptical galaxies.

Subject headings: galaxies: clustering — galaxies: photometry — ultraviolet: general

I. INTRODUCTION

Imagery in the far-ultraviolet (FUV) light is an excellent means to identify the places of active star formation, where young hot stars dominate the emission (Carruthers, Heckathorn, and Opal 1978; Deharveng *et al.* 1980; Donas *et al.* 1981; Bohlin *et al.* 1983; Stecher *et al.* 1982; Hill, Bohlin, and Stecher 1984). It can be a sensitive probe of evolved hot populations in aged stellar systems (Bohlin *et al.* 1985, 1988), as well as of the interstellar dust grains in extended objects (Carruthers and Opal 1977*a*, *b*; Bohlin *et al.* 1982). When the imagery covers a wide field without resolving the structures of individual galaxies, we can survey *total* UV fluxes of individual galaxies resulting from the integration of various components mentioned above (Smith and Cornett 1982).

The number of galaxies whose *total* FUV fluxes are available is, however, very limited at present. *OAO 2* obtained the fluxes at 150 nm for about 20 galaxies (Code and Welch 1979, 1982) within the diaphragm of 10′. Carnochan, Navach, and Wilson (1975) reported the *TD 1* results for five galaxies. The *ANS* provided the UV fluxes for more than 70 galaxies within a limited diaphragm of 2.′5 × 2.′5 (Wesselius *et al.* 1982; de Boer 1982). The *IUE* observations are mostly restricted to the small central part of 20″ ∼ 30″ (Burstein *et al.* 1988).

In a previous paper (Onaka *et al.* 1989, hereafter Paper I), we reported the results of our rocket experiment of the vacuum-ultraviolet (VUV) imagery of the Virgo Cluster region, particularly for bright UV objects. In the present paper we extended the data analysis to faint objects and discuss the properties of the total FUV emission of more than 40 galaxies detected.

The observation was made by the VUV imager GUV aboard the sounding rocket S520-8, which was launched on 1987 February 21 by the Institute for Space and Astronautical Science (ISAS), Japan. The imager GUV consisted of two identical telescopes of 170 mm aperture with different field of view of 4° in diameter. One telescope, GUV1, was directed toward the center of the Virgo Cluster, while the other, GUV2, aimed at the field of 3° south of the center. A combination of a CsI-coated microchannel plate and a resistive anode was used as a detector. One pixel of the detector system corresponded to 2.′4. The total system of the GUV had an effective wavelength $\lambda_0 =$ 156 nm with a passband of the FWHM = 23 nm. Further descriptions of the instrumentation, the absolute calibration, and the observation are given in Paper I.

The present paper deals with the data taken in the *pointing* mode, in which the absolute attitude stability was within 1° and the drift rate of the attitude was less than 0.′5 s^{-1}. The data of one image frame were sent to the ground every 2.52 s. The final pictures were obtained by superposing 70 frames of images with the correction of the attitude variation. The final resolutions were estimated by the Gaussian fit of the image profiles of point sources, being 16.′0 in the right ascension and 8.′2 in the declination (FWHM), independent of the positions on the pictures. The attitude drift was mostly in the right ascension direction, and this may be the explanation for this anisotropy in the resolution.

In the following, we describe the data reduction and the observational results in § II. A comparison of the observed FUV flux with other radiation characteristics of the detected galaxies are made in § III. Finally discussion on the bearings of the present findings is given in § IV. The evaluation of the diffuse FUV background will be reported separately.

II. REDUCTION AND OBSERVATIONAL RESULTS

In order to suppress the small-scale fluctuations, the Gaussian smoothing with a standard deviation of one-half of the image resolution obtained above was applied to the original superposed pictures without significant loss of spatial information. This process enabled us to better determine the sky background and enhanced the image quality, significantly improving the accuracy of the position determination of

© American Astronomical Society • Provided by the NASA Astrophysics Data System

1990ApJ...363..422K

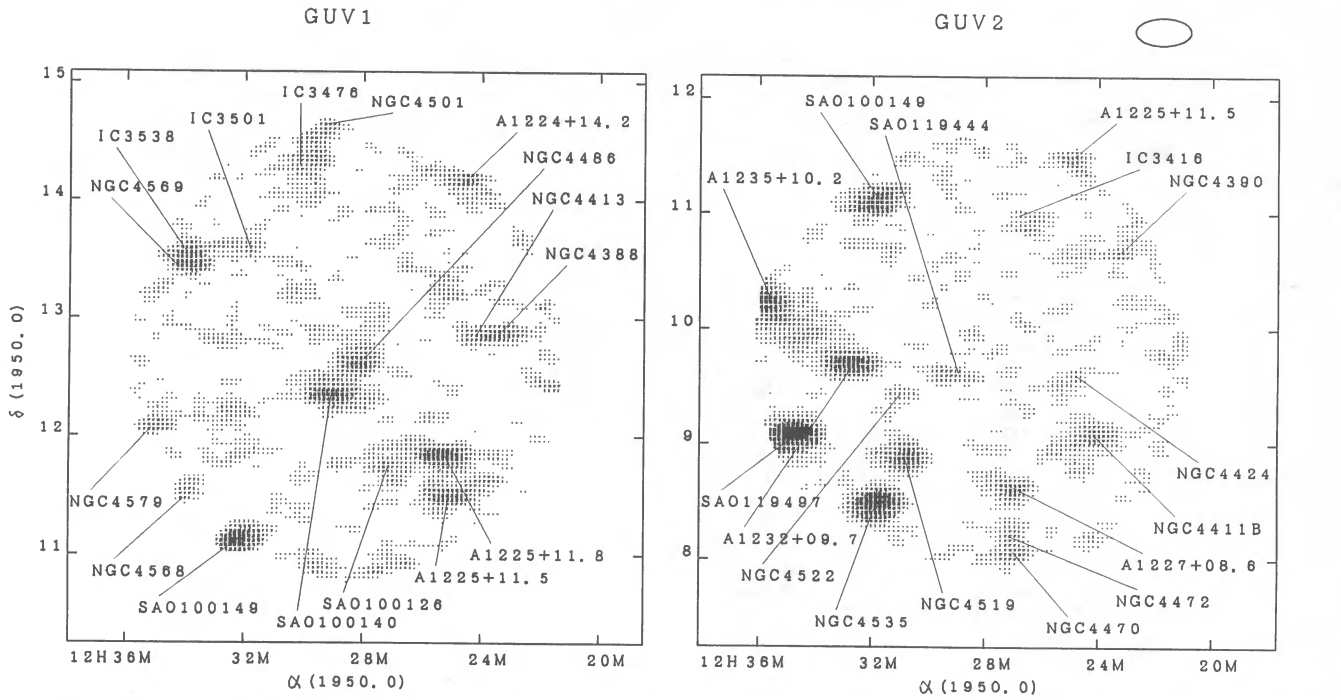

FIG. 1.—The far-ultraviolet images of the central region of the Virgo Cluster. The background has been subtracted. In the upper right corner, the typical size of the integration area is indicated.

prominent objects. The pictures with sky background subtracted are presented in Figure 1. The positions of the prominent objects were determined by iteratively minimizing the differences between the peak positions in the GUV pictures and the optical positions given by SAO Catalog for stars and by Binggeli, Sandage, and Tammann (1985, hereafter BST) for galaxies. The rms deviations of the GUV peak positions of the objects relative to the optical positions were less than 2.4, and the disagreement never exceeded 4.8 except for the objects on the margins of the pictures.

The smoothed pictures made it possible to separate contributions from individual objects overlapping with each others. As an example, NGC 4569, whose image overlapped with IC 3583 and whose flux was not given in Paper I, was clearly identified in the present smoothed picture, and its FUV flux could be derived from the deconvolution of the merged image.

The flux in the area corresponding to a galaxy or to a star was integrated to give the total FUV flux or an upper limit for the respective objects. The typical integration area was an ellipse with axes of 12 pixels × 6 pixels (28.8 × 14.4) as shown in the upper right corner of Figure 1. The background was estimated by the linear interpolation of the radiation in the area surrounding the integration ellipse.

The objects in BST with $B_T < 14$ mag and those detected by *IRAS* (IRAS Point Source Catalog; Helou *et al.* 1988; Knapp *et al.* 1989) were searched for in the GUV pictures. A caveat is that accidental coincidence of the searched objects with unknown UV sources within a circle of about 2.4 in radius could not be ruled out. The accuracy of the obtained fluxes was limited mainly by the fluctuation of the background. The detection limit of the present measurements was found to be about 4–5 × 10^{-15} ergs cm^{-2} s^{-1} Å^{-1}, slightly depending on the positions on the pictures. Upper limits higher than this value are given for some objects because of the presence of brighter sources in their direct vicinity.

The obtained FUV fluxes of galaxies are summarized in Table 1. The data for stars are to be consulted in Paper I. In column (1), the galaxy designations of the identified objects are given in the order of priority, NGC number, IC number, UGC number (Nilson 1973), or VCC number (BST). The total B magnitude in column (2) and the morphological type in column (3) were taken from BST. The FUV flux f_λ (156 nm) obtained by GUV and its error (1 σ) in units of 10^{-14} ergs cm^{-2} s^{-1} Å^{-1} are given in column (4). Column (5) gives the GUV position with an accuracy of about 3′. The optical position in column (6) was adopted from BST. Non-Virgo members are indicated in the notes according to BST. A total of 42 galaxies were detected in the present study, of which 30 were observed for the first time in the FUV region.

The fluxes for bright sources redetermined in this paper are in agreement with those presented in Paper I within the expected accuracy, except for a few sources. In addition to the comments given in Paper I and to the note to Table 1, some comments are included below for several galaxies.

NGC 4406.—This is one of the optically brightest galaxies in the cluster. In its vicinity there are NGC 4402 and NGC 4387 whose FUV fluxes were detected. No FUV flux enhancement over the detection limit was recognized at the position of NGC 4406. *IUE* observations (Burstein *et al.* 1988) showed a fair amount of the FUV flux in the central part of the galaxy (see Table 3). The FUV flux in NGC 4406 might be concentrated toward the center more strongly than suggested for NGC 4472 and NGC 4486 (Paper I).

IC 3371.—This source should have been detected both in GUV1 and GUV2. While the detection by GUV1 was secure, the GUV2 picture showed a marginal signal (~3 × 10^{-15} ergs cm^{-2} s^{-1} Å^{-1}) at the source position.

NGC 4535.—Paper I reported the FUV flux of 1.84 × 10^{-13} ergs cm^{-2} s^{-1} Å^{-1} for NGC 4535. This source is located on the margin of the GUV2 picture, and the refined analysis of the background led to a somewhat smaller flux.

NGC 4458/NGC 4461.—The difference in position between

© American Astronomical Society • Provided by the NASA Astrophysics Data System

1990ApJ...363..422K

TABLE 1

ULTRAVIOLET FLUXES OF GALAXIES BY GUV

NAME (1)	B_T (2)	TYPE (3)	f_λ (156 nm) (10^{-14} ergs cm^{-2} s^{-1} Å^{-1}) (4)	POSITION (1950) GUV α, δ (5)	POSITION (1950) Optical α, δ (6)
IC 3255	14.6	Sbc(s)II	1.22 ± 0.36	$12^h21^m.0$, 09°54′	$12^h21^m.0$, 09°55′
IC 3258	13.75	ScIII–IV	0.45 ± 0.23	12 20.9, 12 45	12 21.2, 12 45
NGC 4351	13.04	Sc(s)II.3	1.85 ± 0.37	12 21.6, 12 28	12 21.5, 12 29
NGC 4356	14.04	Sc (on edge)	<0.4	...	12 21.7, 08 49
NGC 4360	13.47	E2	0.56 ± 0.34	12 21.8, 09 31	12 21.8, 09 34
NGC 4371	11.80	$SB0_2(r)(3)$	<0.5	...	12 22.4, 11 59
NGC 4374	10.26	E1	0.60 ± 0.32	12 22.5, 13 11	12 22.5, 13 10
NGC 4380	12.36	Sab(s)	1.82 ± 0.40	12 22.9, 10 19	12 22.8, 10 18
NGC 4387	13.02	E5	0.54 ± 0.27	12 23.1, 13 10	12 23.2, 13 05
NGC 4388	11.83	Sab	2.50 ± 0.45	12 23.4, 12 55	12 23.2, 12 56
NGC 4390	13.27	Sbc(s)II	1.12 ± 0.43	12 23.2, 10 42	12 23.3, 10 44
NGC 4402	12.56	Sc (on edge)	1.08 ± 0.46	12 23.6, 13 22	12 23.6, 13 23
NGC 4406	10.06	$S0_1(3)$/E3	<0.4	...	12 23.7, 13 13
NGC 4410	14.15	pec	<0.4	...	12 23.9, 09 18
NGC 4413	12.97	SBbc(rs)II–III	1.94 ± 0.39	12 24.2, 12 54	12 24.0, 12 53
NGC 4415	13.72	d:E1,N	<0.4	...	12 24.1, 08 43
NGC 4416	12.89	SBc(s)II.2	0.79 ± 0.34	12 24.3, 08 13	12 24.2, 08 12
NGC 4411B	12.92	Sc(s)II	3.70 ± 0.47	12 24.1, 09 07	12 24.3, 09 10
NGC 4417	12.08	$S0_1(7)$	<0.4	...	12 24.3, 09 52
IC 3355	14.82	SBmIII	<0.5	...	12 24.3, 13 27
NGC 4424	12.32	Sa pec	1.22 ± 0.41	12 24.8, 09 39	12 24.7, 09 42
NGC 4425	12.82	SBa	<0.6	...	12 24.7, 13 01
IC 3371	15.32	Sc (on edge)	0.63 ± 0.36	12 24.9, 11 08	12 24.8, 11 09
NGC 4429	11.15	$S0_3(6)$/Sa pec	<0.4	...	12 24.9, 11 23
NGC 4431	13.72	dS0(5),N	<0.4	...	12 24.9, 12 34
NGC 4434	12.99	$E0/S0_1(0)$	<0.4	...	12 25.1, 08 26
NGC 4435	11.84	$SB0_1(6)$	0.80 ± 0.30	12 25.0, 13 24	12 25.1, 13 21
NGC 4438	10.91	Sb (tides)	1.00 ± 0.34	12 25.3, 13 15	12 25.2, 13 17
NGC 4440	12.74	SBa(sr)	<0.4	...	12 25.4, 12 34
NGC 4442	11.40	$SB0_1(6)$	<0.5	...	12 25.5, 10 05
NGC 4446	14.41	Sc(s)II.2	<0.7	...	12 25.6, 14 11
NGC 4447	14.69	$RSB0_1(3)$	<0.7	...	12 25.7, 14 11
NGC 4445	13.66	S (on edge)	<0.4	...	12 25.7, 09 43
UGC 7590	14.6	Sbc(s)I.8	0.82 ± 0.32	12 25.7, 09 00	12 25.8, 09 00
NGC 4451	13.31	Sc(s)III	<0.4	...	12 26.1, 09 32
NGC 4452	13.30	$S0_1(9)$	<0.6	...	12 26.2, 12 02
NGC 4458	12.92	E1	0.75 ± 0.42	12 26.5, 13 29	12 26.4, 13 31
NGC 4459	11.37	$S0_3(2)$	0.81 ± 0.41	12 26.5, 14 13	12 26.5, 14 15
NGC 4461	12.09	Sa	<0.5	...	12 26.5, 13 28
VCC 1174	15.5	BCD?	<0.5	...	12 26.8, 10 13
NGC 4464	13.70	E3	<0.4	...	12 26.8, 08 26
NGC 4469	12.22	Sa	<0.4	...	12 26.9, 09 02
NGC 4466	14.62	Sc:	<0.4	...	12 27.0, 07 58
NGC 4468	13.80	S0/a	<0.5	...	12 27.0, 14 20
IC 3416	14.78	ImIII	1.01 ± 0.40	12 27.0, 11 05	12 27.0, 11 04
NGC 4470	13.04	ScIII pec	3.08 ± 0.42	12 27.0, 08 07	12 27.1, 08 06
NGC 4472	9.31	$E2/S0_1(2)$	2.11 ± 0.42	12 27.2, 08 15	12 27.2, 08 17
NGC 4473	11.10	E5	0.72 ± 0.37	12 27.3, 13 42	12 27.3, 13 42
NGC 4474	12.60	$S0_1(8)$	<0.5	...	12 27.4, 14 21
IC 3425	14.31	Sb(s)I–II	0.73 ± 0.34	12 27.4, 10 56	12 27.4, 10 53
NGC 4476	13.14	$S0_3(5)$	<0.5	...	12 27.5, 12 38
NGC 4477	11.31	$SB0_{1/2}$/SBa	<0.6	...	12 27.5, 13 55
NGC 4482	13.68	d:E5,N	<0.4	...	12 27.6, 11 03
NGC 4478	12.15	E2	<0.5	...	12 27.8, 12 36
NGC 4479	13.45	$SB0_2(2)$	<0.5	...	12 27.8, 13 51
NGC 4486B	15.11	E1	<0.5	...	12 28.0, 12 46
NGC 4483	13.17	$SB0_1(5)$	<0.5	...	12 28.1, 09 18
NGC 4486	9.58	E0	4.30 ± 0.48	12 28.1, 12 40	12 28.3, 12 40
NGC 4488	12.86	S0 pec(tides)	<0.4	...	12 28.3, 08 38
NGC 4491	13.43	SBa(s)	<0.4	...	12 28.4, 11 46
NGC 4486A	13.5:	E2	<0.5	...	12 28.4, 12 33
NGC 4492	13.17	Sa (dust arms)	<0.5	...	12 28.5, 08 21
NGC 4497	13.34	SB0(5)/SBa	1.09 ± 0.34	12 28.9, 11 49	12 29.0, 11 54
IC 3457	14.43	dE3,N	0.55 ± 0.32	12 29.5, 12 56	12 29.3, 12 56
NGC 4501	10.27	Sbc(s)II	2.41 ± 0.51	12 29.3, 14 41	12 29.5, 14 42
NGC 4503	12.12	Sa	0.82 ± 0.40	12 29.6, 11 27	12 29.6, 11 27
NGC 4506	13.64	S pec (dust)	<0.5	...	12 29.7, 13 42
IC 3468	13.81	E1,N:	<0.5	...	12 29.7, 10 32

© American Astronomical Society • Provided by the NASA Astrophysics Data System

1990ApJ...363..422K

TABLE 1—*Continued*

Name (1)	B_T (2)	Type (3)	f_λ (156 nm) (10^{-14} ergs cm^{-2} s^{-1} Å^{-1}) (4)	Position (1950) GUV α, δ (5)	Position (1950) Optical α, δ (6)
VCC 1437	15.7	BCD	<0.4	...	12 30.0, 09 27
IC 3475	13.93	ImIV	<0.5	...	12 30.1, 13 03
IC 3476	13.29	Sc(s)II.2	2.40 ± 0.7	12 29.5, 14 24	12 30.2, 14 20
IC 3483	15.3	S pec,N	0.84 ± 0.37	12 30.5, 11 35	12 30.7, 11 37
NGC 4519	12.34	SBc(rs)II.2	7.80 ± 0.55	12 30.8, 08 55	12 31.0, 08 56
NGC 4522	12.73	Sc/Sb:	1.33 ± 0.32	12 31.0, 09 29	12 31.1, 09 27
IC 3501	14.51	d:E1	1.40 ± 0.42	12 31.6, 13 37	12 31.3, 13 36
NGC 4526	10.61	$S0_3(6)$	<0.4	...	12 31.5, 07 59
NGC 4528	12.70	$SB0_2(5)$	<0.6	...	12 31.6, 11 36
NGC 4531	12.58	Sa pec	<0.5	...	12 31.7, 13 21
NGC 4535	10.51	SBc(s)I.3	14.80 ± 0.64	12 31.8, 08 32	12 31.8, 08 29
VCC 1579	14.87	S0:	<0.4	...	12 32.2, 09 17
NGC 4550	12.50	$E7/S0_1(7)$	<0.5	...	12 33.0, 12 30
NGC 4551	12.85	E2	<0.5	...	12 33.1, 12 32
NGC 4552	10.78	$S0_1(0)$	1.62 ± 0.48	12 33.0, 12 51	12 33.1, 12 50
NGC 4564	12.02	E6	0.93 ± 0.46	12 34.0, 11 41	12 33.9, 11 43
NGC 4568	11.70	Sc(s)III	4.68 ± 0.46	12 34.1, 11 30	12 34.0, 11 31
IC 3583	13.91	SmIII	3.51 ± 0.47	12 34.0, 13 36	12 34.2, 13 32
NGC 4569	10.25	Sab(s)I–II	3.51 ± 0.47	12 34.3, 13 29	12 34.3, 13 26
NGC 4578	12.22	$S0_{1/2}(4)$	<0.5	...	12 35.0, 09 50
NGC 4579	10.56	Sab(s)II	2.48 ± 0.44	12 35.1, 12 06	12 35.2, 12 06

Notes on Individual Objects.—IC 3255: not a member of the Virgo Cluster; IC 3258: on the edge of the field of view of GUV1; NGC 4360: not a member of the Virgo Cluster; NGC 4374: A1221+12.7 overlaps; NGC 4387: NGC 4402 overlaps; NGC 4388: NGC 4413 overlaps; NGC 4402: NGC 4406 and NGC 4387 overlap; NGC 4406: NGC 4402 overlaps; NGC 4410: A and B components. Not a member of the Virgo Cluster; NGC 4413: NGC 4388 overlaps; NGC 4415: A1224+08.8 overlaps; NGC 4411B: NGC 4411A is included; NGC 4425: NGC 4413 overlaps; NGC 4429: A1225+11.5 overlaps; NGC 4435: NGC 4438 overlaps; NGC 4446: A1224+14.2 overlaps. Not a member of the Virgo Cluster; NGC 4447: Not a member of the Virgo Cluster; NGC 4452: A1225+11.8 overlaps; NGC 4458: inseparable from NGC 4461; NGC 4461: NGC 4458 overlaps; NGC 4466: NGC 4470 overlaps; IC 3425: not a member of the Virgo Cluster; NGC 4476: NGC 4486 overlaps; NGC 4478: NGC 4486 overlaps; NGC 4486A: SAO 100140 overlaps; IC 3457: marginal detection; IC 3476: tentative identification; IC 3483: IC 3481 overlaps; NGC 4526: on the edge of the field of view of GUV2; VCC 1579: not a member of the Virgo Cluster; NGC 4564: NGC 4567 and NGC 4568 overlap; NGC 4568: NGC 4564 overlaps. NGC 4567 is included; IC 3583: NGC 4569 overlaps; NGC 4569: IC 3583 overlaps.

these two objects is only 3′, and GUV could not spatially resolve them. Judging from the peak position and the brightness in the near-UV (Smith and Cornett 1982), we assigned all the flux measured to NGC 4458, but a partial contribution from NGC 4461 could not be ruled out.

IC 3457.—A marginal enhancement was detected at the position of this dwarf elliptical with a nucleus, whose near-UV flux was also detected by Smith and Cornett (1982).

IC 3476.—This is a bright source in FIR and near-UV, but GUV did not detect an unambiguous flux centered at the exact source position. There is, however, a bright source close to IC 3476, and we tentatively identify this as IC 3476 in spite of the position difference larger than the expected error.

IC 3501.—This is classified as a probable dwarf E in BST with the type index $T = -6$:, and no further information was available for its UV or IR properties. The agreement in position is marginal, and the identification needs confirmation.

IC 3583.—In Paper I, the FUV flux of IC 3583 was reported to be 7.0×10^{-14} ergs cm^{-2} s^{-1} Å^{-1}. In the present refined analysis, NGC 4569 was found to overlap with IC 3583. From a simple deconvolution, one-half of the flux turned out to come from NGC 4569.

Since there were marginal identifications for two dwarf ellipticals fainter than $B_T = 14.0$ (IC 3457 and IC 3501), we searched for enhancements at the positions of other dwarf ellipticals, in particular, those with a nucleus, but failed to confirm any detection of the other sources with the flux level stronger than 5×10^{-15} ergs cm^{-2} s^{-1} Å^{-1}. The flux from IC 3478 (dE2, N; $B_T = 14.34$) might overlap with the IC 3476 image, but we could not confirm it with certainty.

An enhancement of the FUV flux was recognized but no optical counterpart was found in catalogs at some positions. The fluxes of these anonymous sources are given in Table 4 of Appendix A with their GUV positions.

One should keep it in mind that the observed FUV fluxes in Tables 1 and 4 are still not corrected either for the Galactic absorption or for the internal absorption in the source galaxies. Since we observed rather a small area in the sky, the differences in the Galactic absorption may be ignored in the comparative study of FUV properties among the observed galaxies.

III. CORRELATION WITH RADIATIONS IN OTHER WAVELENGTH RANGES

In this section, the observed FUV flux of galaxies are compared with the fluxes in other wavelength ranges published by various investigators. The data compared are summarized in Table 2 for the UV, visual, H I 21 cm, far-infrared, X-ray, and radio continuum fluxes. All of the data except for the type index in Table 2 are given in the logarithm with the base of 10. The FUV flux corrected for the intrinsic absorption in each galaxy, $f_{\lambda,c}$ (156 nm), is also given in Table 2. The extinction

© American Astronomical Society • Provided by the NASA Astrophysics Data System

1990ApJ...363..422K

TABLE 2

FUV, OPTICAL, X-RAY, AND RADIO DATA OF THE INVESTIGATED VIRGO GALAXIES

Name[a] (1)	T[b] (2)	(156)[c] (3)	$(156)_c$[d] (4)	(156)/(550)[e] (5)	(242)/(550)[f] (6)	H I 21 cm[g] (7)	FIR[h] (8)	X-Ray[i] (9)	Radio[j] (10)
IC 3255	4:	−13.91	...	...	...	...	...	...	...
IC 3258	9	−14.35	−14.32	−0.42	0.17	0.57	−13.49	...	...
NGC 4351	2	−13.73	−13.50	−0.24	−0.50	0.62	−13.30	...	...
NGC 4356	5:	< −14.40	...	< −0.87	−1.27	...	−13.44	...	...
NGC 4371	−1	< −14.30	< −14.24	< −1.57	−1.84	<0.48	< −14.48	...	...
NGC 4374	−5	−14.22	−14.22	−2.10	−1.33	<0.34	−13.53	40.65	3.86
NGC 4380	3	−13.74	−13.67	−0.65	−0.91	0.48	−13.22	...	−0.70
NGC 4387	−5	−14.27	...	−0.99	< −1.65	...	< −14.43	...	1.26
NGC 4388	3	−13.60	−13.35	−0.70	−0.87	0.81	−12.22	...	2.16
NGC 4390	4	−13.95	−13.55	−0.32	−0.22	0.85	−13.29	...	...
NGC 4402	3	−13.97	−13.64	−0.75	−0.93	0.90	−12.39	...	...
NGC 4406	−5	< −14.40	< −14.40	< −2.42	−1.71	<0.40	−13.26	41.44	0.04
NGC 4413	3	−13.71	−13.56	−0.35	−0.77	0.53	−13.15	...	...
NGC 4415	0	< −14.40	< −14.26	...	...	<0.23	...	...	...
NGC 4416	3	−14.10	−13.84	−0.58	< −1.41	0.68	−13.17	...	...
NGC 4411B	8	−13.43	−13.23	0.06	−0.31	1.34	−13.27	...	...
NGC 4417	−2	< −14.40	< −14.12	< −1.56	−1.47	0.76	< −14.56	...	...
IC 3355	10	< −14.30	...	...	...	0.37	...	...	...
NGC 4424	1	−13.91	−13.84	−0.83	−0.98	0.45	−12.78	...	...
NGC 4425	−2	< −14.22	< −14.02	< −1.00	−1.63	<0.42	< −14.42	...	...
IC 3371	5:	−14.20	...	...	...	...	...	...	...
NGC 4429	−1	< −14.40	< −14.35	< −1.96	−2.15	<0.45	−12.96	...	...
NGC 4431	−2	< −14.40	...	< −0.68	< −1.21	...	...	...	...
NGC 4434	−5	< −14.40	...	...	...	...	< −14.49	...	...
NGC 4435	−2	−14.10	−14.00	...	...	<0.46	−12.92	...	...
NGC 4438	0	−14.00	−13.95	...	...	0.89	−12.57	...	2.06
NGC 4440	1	< −14.40	< −14.34	< −1.23	−1.74	<0.08	< −13.92	...	...
NGC 4442	−2	< −14.30	< −14.21	< −1.71	−1.71	<0.51	−14.13	...	...
NGC 4445	2	< −14.40	< −14.16	< −0.81	−1.55	−0.02	−13.59	...	...
UGC 7590	4:	−14.09	−13.17	...	...	1.19	...	...	...
NGC 4451	−2	< −14.40	< −14.11	< −0.90	−0.77	0.43	−12.94	...	...
NGC 4452	1	< −14.22	< −14.07	< −1.02	−0.11	< −0.19	< −14.67	...	...
NGC 4458	−5	−14.12	−14.12	−0.85	−0.87	<0.38	< −14.57	...	...
NGC 4459	−1	−14.09	−14.03	−1.51	−1.51	<0.53	−12.93	39.98	...
NGC 4461	−1	< −14.30	< −14.18	< −1.42	−1.58	<0.49	< −14.82	...	...
VCC 1174	...	< −14.30	...	...	...	...	−13.70	...	...
NGC 4464	0	< −14.40	...	...	...	...	< −14.23	...	...
NGC 4469	0	< −14.40	< −14.29	< −1.48	−2.02	<0.43	−13.14	...	...
NGC 4466	2	< −14.40	< −13.86	...	...	0.32	...	...	...
NGC 4468	−2	< −14.30	< −13.77	...	...	0.81	< −14.57	...	...
IC 3416	10:	−14.00	−13.99	...	...	< −0.40	...	...	...
NGC 4470	1	−13.51	−12.89	...	...	0.92	−12.95	...	...
NGC 4472	−5	−13.68	−13.68	−1.86	−1.58	< −0.15	< −14.48	41.58	2.36
NGC 4473	−5	−14.14	−14.14	−1.62	−2.02	<0.38	< −14.49	39.92	0.34
NGC 4474	−2	< −14.30	< −14.13	< −1.23	−1.35	<0.38	< −14.59	...	...
NGC 4476	−3	< −14.30	...	< −0.98	−1.64	...	−13.37	...	...
NGC 4477	−2	< −14.22	< −14.19	< −1.60	−1.62	<0.35	−13.46	40.00	...
NGC 4482	−6:	< −14.40	...	...	...	...	...	...	...
NGC 4478	−5	< −14.30	< −14.30	...	...	<0.34	< −14.65	...	...
NGC 4479	−2	< −14.30	< −14.19	< −0.78	−0.87	<0.23	< −14.60	...	...
NGC 4486B	−6	< −14.30	...	...	...	...	< −14.62	...	...
NGC 4483	0	< −14.30	...	< −0.99	< −1.62	...	< −14.08	...	...
NGC 4486	−4	−13.37	...	−1.39	−1.51	...	−13.76	43.76	5.36
NGC 4488	0	< −14.40	...	< −1.08	−1.36	...	−14.13	...	...
NGC 4491	1	< −14.40	< −14.32	< −0.90	−1.15	< −0.11	−12.91	...	...
NGC 4486A	10	< −14.30	...	...	...	...	< −14.34	...	...
NGC 4492	1	< −14.30	< −14.27	< −1.11	−1.70	−0.11	...	...	...
NGC 4497	0	−13.96	...	−0.54	< −1.51	...	< −14.35	...	...
IC 3457	−5	−14.26	...	−0.01	−0.46	...	...	...	...
NGC 4501	3	−13.62	−13.40	−1.36	−0.66	1.53	−11.84	...	2.44
NGC 4503	−3	−14.09	−13.93	−1.22	−1.59	<0.63	< −14.46	...	...
NGC 4506	1	< −14.30	...	< −0.65	−0.36	...	...	...	...
IC 3468	−5:	< −14.30	...	...	...	...	...	...	...
VCC 1437	...	< −14.40	...	...	...	0.12	−13.95	...	...
IC 3475	−5	< −14.30	< −14.30	< −0.25	−0.69	< −0.29	< −13.97	...	...
IC 3476	10	−13.62	−13.60	−0.06	−0.30	0.66	−13.00	...	...
IC 3483	3	−14.08	−13.55	...	...	−0.17	...	...	...
NGC 4519	7	−13.11	−12.66	0.17	−0.35	1.71	−12.66	...	0.96
NGC 4522	6	−13.88	−13.57	−0.48	−0.73	0.85	−12.98	...	1.34
IC 3501	−6:	−13.85	...	...	...	...	...	...	...
NGC 4526	−2	< −14.40	...	< −2.08	−1.93	...	−12.42	...	...

© American Astronomical Society • Provided by the NASA Astrophysics Data System

1990ApJ...363..422K

TABLE 2—*Continued*

Name[a] (1)	T[b] (2)	(156)[c] (3)	$(156)_c$[d] (4)	(156)/(550)[e] (5)	(242)/(550)[f] (6)	H I 21 cm[g] (7)	FIR[h] (8)	X-Ray[i] (9)	Radio[j] (10)
NGC 4528	−3	< −14.22	...	< −1.08	−1.20	...	< −14.52	...	...
NGC 4531	1	< −14.30	< −14.29	< −1.23	−1.46	−0.60	−13.43	...	...
NGC 4535	5	−12.83	−12.50	−0.36	−0.49	1.95	−12.07	...	1.81
NGC 4550	−1	< −14.30	< −14.27	< −1.26	−1.05	<0.61	−14.14	<39.80	...
NGC 4551	−5	< −14.30	< −14.30	< −1.11	−1.52	0.34	< −14.53	...	1.26
NGC 4552	−5	−13.79	−13.79	−1.44	−1.43	<0.40	−13.95	40.53	1.86
NGC 4564	−5	−14.03	−14.03	−1.22	−1.54	< −0.55	< −14.39	<39.70	1.06
NGC 4568	4	−13.33	−12.96	...	...	1.33	−11.86	...	...
IC 3583	10	−13.45	−13.43	...	...	0.52	−13.41	...	...
NGC 4569	2	−13.45	−13.40	−1.18	−0.69	1.09	−12.18	...	1.92
NGC 4578	−2	< −14.30	< −14.30	< −1.31	−1.98	< −0.55	< −14.63	...	...
NGC 4579	3	−13.61	−13.54	−1.33	−1.09	0.95	−12.34	...	2.01

[a] Name of the galaxy.
[b] Type index. The colon indicates those estimated from the classification by BST.
[c] Logarithm of f_λ (156 nm) in ergs cm^{-2} s^{-1} Å^{-1}.
[d] Logarithm of $f_{\lambda,c}$ (156 nm), the FUV flux in ergs cm^{-2} s^{-1} Å^{-1} for which the internal extinction is corrected (see text).
[e] Logarithm of f_λ (156 nm)/f_λ (550 nm).
[f] Logarithm of f_λ (242 nm)/f_λ (550 nm).
[g] Logarithm of H I 21 cm flux in Jy km s^{-1}.
[h] Logarithm of far-infrared flux in W m^{-2}.
[i] Logarithm of X-ray luminosity in ergs s^{-1}.
[j] Logarithm of radio flux at 1.4 or 1.5 GHz in mJy.

correction was made according to Donas and Deharveng (1984) and Donas *et al.* (1987) by using the H I 21 cm flux. The value of $A_\lambda/E(B-V)$ at 150 nm was assumed to be 8.0 for galaxies of $T \leq 3$, 8.1 for $T = 4$ and 5, 8.2 for $T = 6$ and 7, and 8.5 for $T \geq 8$, where T is the morphological type index. The correction may be subject to large uncertainties which could be up to 1 mag (Donas and Deharveng 1984). Because of the uncertainties, the following correlation studies are made for the observed FUV flux. The conclusions hardly change even if the corrected FUV flux is applied, insofar as we are not concerned with absolute amounts. The non-Virgo members in Table 1 are excluded from the analysis in this section.

Figure 2 shows the correlation of the ratio of the FUV flux f_λ (156 nm) to the flux in the visual region f_λ (550 nm) taken

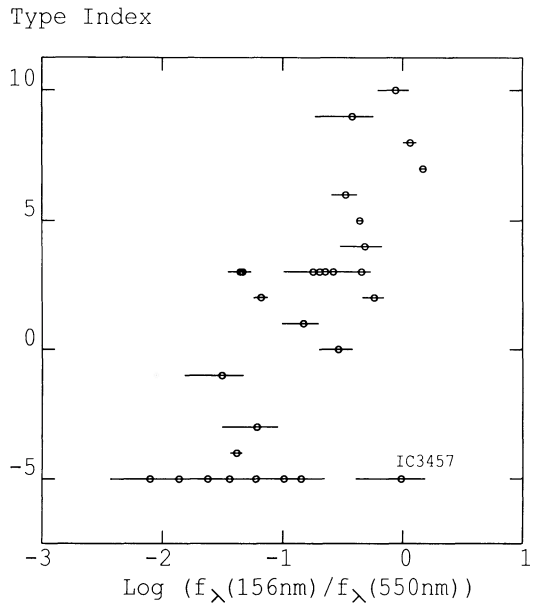

FIG. 2.—The dependence of the far-ultraviolet excess on the morphological type index of galaxies.

from Watanabe (1983) with the type index of galaxies, T, given in de Vaucouleurs, de Vaucouleurs, and Corwin (1976, hereafter RC2). The average ratio of the FUV flux to the visual flux for late-type galaxies of $6 \leq T \leq 10$ is about 20 times higher than that for the bulk of early-type galaxies of $T = -4$ and -5. The early- to middle-type spiral galaxies of $0 \leq T \leq 5$ fall in between. The early-type galaxies ($T < 0$) show more scatter than the spirals ($T \geq 0$) do. This is the same trend as noted in near-UV observation (Smith and Cornett 1982). The galaxy IC 3457 showing the highest ratio among the galaxies of $T = -5$ is a dwarf elliptical with a nucleus (BST). This fact suggests that the nucleus may play an important role in the FUV radiation of E galaxies, though the FUV detection of IC 3457 is marginal.

A two-color diagram, log [f_λ (242 nm)/f_λ (550 nm)] versus log [f_λ (156 nm)/f_λ (550 nm)] is presented in Figure 3. The values of the UV flux at $\lambda = 242$ nm were adopted from Smith and Cornett (1982). Roughly speaking, the plots are distributed along a sequence of increasing type index from lower left to upper right in Figure 3. At least for spiral galaxies, the sequence can be interpreted as a result of changing ratio of young hot stars to old cool stars, due to varying star formation activity. It is conspicuous that the dwarf elliptical with a nucleus, IC 3457, is located close to the upper end of the sequence, indicating possible star-forming activity in the nuclear region of this galaxy.

In contrast to the behavior of spiral galaxies, the majority of early-type galaxies of $T < 0$ are distributed rather flat in Figure 3. This is apparently a reflection of the varying "FUV turn-up" in the energy spectra of ellipticals found by Code and Welch (1979; *OAO 2*) and confirmed by Bertola, Cappaccioli, and Oke (1982; *IUE*). This finding suggests that, among galaxies of early type, the number of "hot" stars responsible for the FUV flux may vary independently from the number of "warm" stars responsible for the UV flux at 242 nm, not alike in the case of spiral galaxies.

The integrated flux of the H I 21 cm line adopted from various sources (Helou *et al.* 1981; Helou, Huffman, and Salpeter 1984; Huffman *et al.* 1987, 1989; Huchtmeier and

© American Astronomical Society • Provided by the NASA Astrophysics Data System

1990ApJ...363..422K

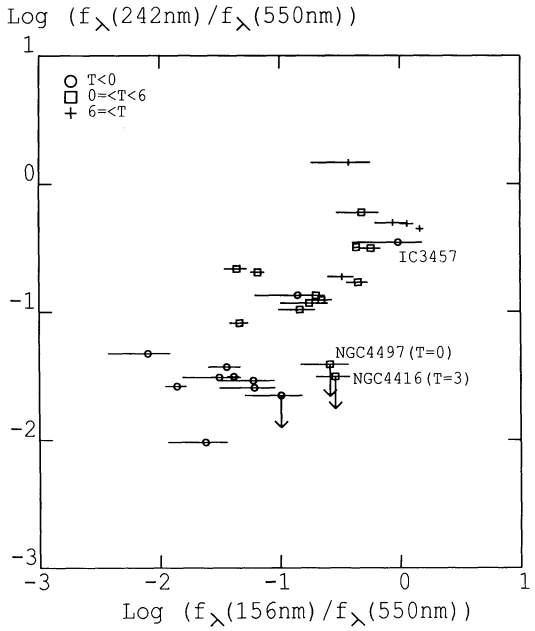

FIG. 3.—Two-color diagram of the observed Virgo galaxies

Richter 1986) is plotted against the FUV flux in Figure 4 for galaxies of $T \geq 0$. The majority of spiral galaxies are distributed along a sequence, indicating roughly a linear proportionality between both quantities. The regression line analysis resulted in log f(H I 21 cm) (in Jy km s^{-1}) = 0.80 log f_λ (156 nm) (in ergs cm^{-2} s^{-1} Å^{-1}) + 11.82 with a correlation coefficient of 0.62. This fact supports the general idea that the FUV radiation of spirals is related to star formation activity. Most early-type galaxies of $T < 0$ are below the border of the detection of the H I 21 cm flux. In the specific case of NGC 4472, the observed H I 21 cm flux is definitely less than that expected from the FUV flux if this should be tightly related to the star formation in the same sense as in spiral galaxies.

We examine the correlation between the FUV flux and the far-infrared (FIR) flux in Figure 5. The plotted FIR flux was taken from *IRAS* catalogs (Jura *et al.* 1987; Helou *et al.* 1988; Knapp *et al.* 1989), derived from f_ν (60 μm) and f_ν (100 μm) according to Helou *et al.* (1988). This figure shows essentially the same trend as Figure 4, but with a larger scatter than the latter for spiral galaxies. Part of the increased scatter seems to be caused by the enhancement of the FIR flux in some of early-type spiral galaxies relative to the H I 21 cm flux. Such an enhancement in the FIR flux may be caused by the excess of dust relative to H I gas in these galaxies.

We have plotted also the CO 2.6 mm flux for late-type galaxies adopted from Kenny and Young (1986) and Stark *et al.* (1986) against the FUV flux, finding essentially the same trend as in the upper part of Figure 5, indicating the physical interrelation between the star formation activity and the richness in dust and molecules in late-type galaxies.

Figure 6 shows the correlation between the observed FUV flux and the X-ray luminosity (0.2–2 keV) observed from *Einstein* (Forman, Jones, and Tucker 1985) for early-type galaxies. The distance to the Virgo Cluster was taken as 21.9 Mpc (Kennicutt 1983*a*). When the anomalously low FUV flux of NGC 4406 is ignored, we find a relation $L_X \propto f_\lambda^\alpha$ (156 nm) with $\alpha = 3.2 \pm 0.9$ and with a correlation coefficient of 0.82 ± 0.4, depending upon whether the extreme case NGC 4486 is included or not. The X-ray luminosity of NGC 4486 may include part of the flux of the cluster origin, and it may be regarded as a different class. If we exclude NGC 4486 and take NGC 4406 into account, the clear correlation disappears between the two quantities.

According to Fabbiano, Trinchieri, and Macdonald (1984) and Fabbiano and Trinchieri (1985), the X-ray flux of spiral galaxies can be explained by the contributions from discrete sources. On the other hand, the X-ray luminosity from early-

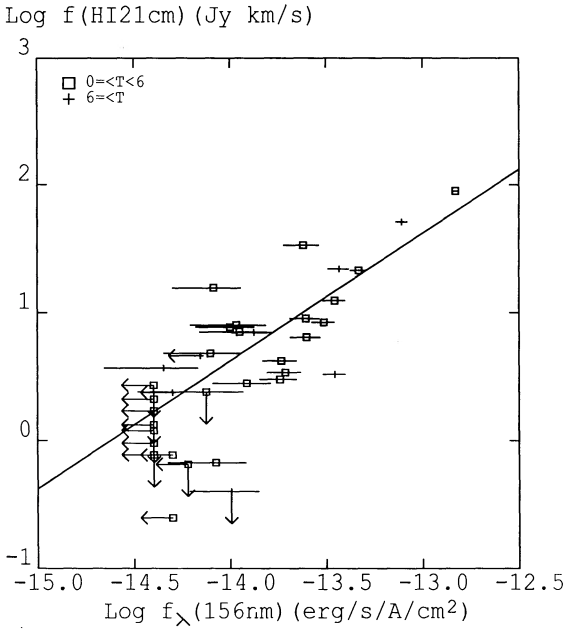

FIG. 4.—The correlation of the far-ultraviolet flux with the H I 21 cm flux for the Virgo spiral galaxies. A linear relation, f(H I 21 cm) $\propto f_\lambda$ (156 nm), is indicated by a line.

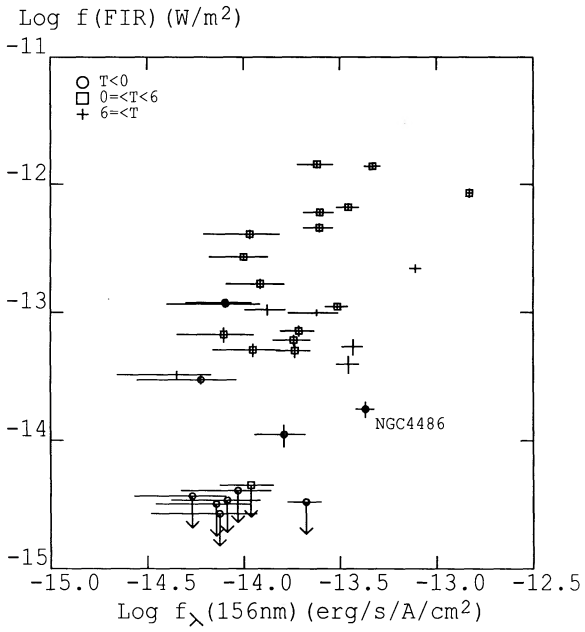

FIG. 5.—The correlation of the far-ultraviolet flux with the far-infrared flux for the Virgo spiral galaxies. The latter is the weighted mean of the flux densities at 60 and 100 μm (Helou *et al.* 1988).

© American Astronomical Society • Provided by the NASA Astrophysics Data System

1990ApJ...363..422K

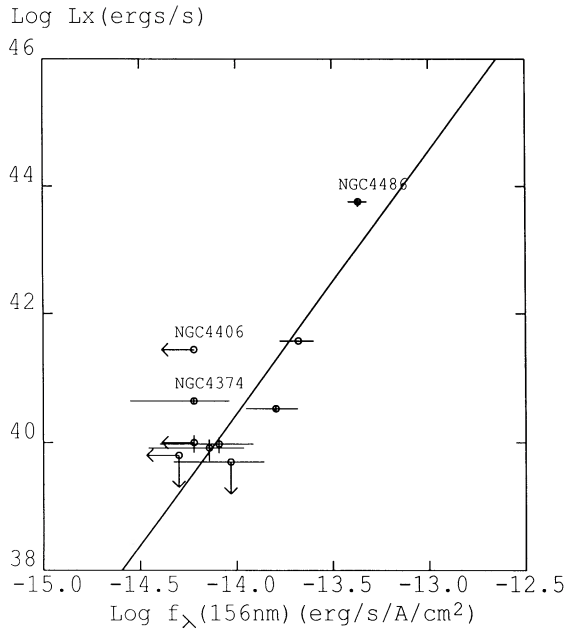

FIG. 6.—The correlation of the far-ultraviolet flux with the X-ray luminosity in 0.2–2 keV band for the Virgo ellipticals. A straight line shows the regression line log $L_X = 4.1 \log f_\lambda$ (156 nm) + 57.9, with a correlation coefficient of 0.86.

type galaxies may be divided into the diffuse extended component and the contribution from discrete sources, the latter being supposed to be proportional to the total blue luminosity of the galaxy (Canizares, Fabbiano, and Trinchieri 1987; Fabbiano, Gioia, and Trinchieri 1989). Following Canizares, Fabbiano, and Trinchieri (1987), we subtracted the part of the X-ray luminosity proportional to the blue luminosity from the observed luminosity for early-type galaxies and plotted the modified X-ray luminosity ΔL_X versus the FUV flux. The correlation turned out to be $\Delta L_X \propto f_\lambda^\alpha$ (156 nm) with $\alpha = 3.6 \pm 0.9$ and with a correlation coefficient of 0.82 ± 0.05, not changing the basic trends of Figure 6.

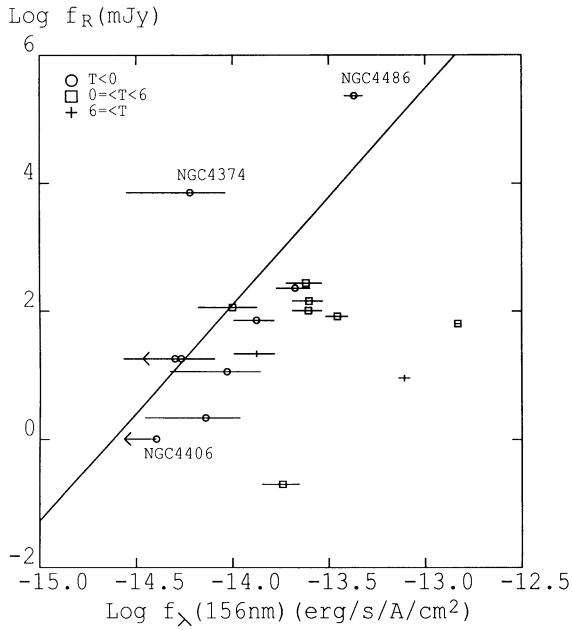

FIG. 7.—The correlation of the far-ultraviolet flux with the radio continuum flux at 1.4–1.5 Hz band for the Virgo galaxies. The straight line shows a relation $f_R = 3.4 \log f_\lambda$ (156 nm) + 2.1 with a correlation coefficient of 0.63 for elliptical galaxies.

When we plotted the continuum radio flux at 1.4 or 1.5 GHz, f_R, adopted from Condon (1987), Condon, Yin, and Burstein (1987), and Bender *et al.* (1989) against the FUV flux in Figure 7, we found a tight relation $f_R \propto f_\lambda^\beta$ (156 nm) with $\beta = 4.9$ and with a correlation coefficient of 0.91 for galaxies of $T < 0$, if NGC 4374 is excluded. When NGC 4374 is included, we find $\beta = 3.4$ with a correlation coefficient of 0.63. The cause of the radiation around 1.5 GHz is generally considered to be nuclear activity for ellipticals and to be supernova activity for spirals (Bender *et al.* 1989; Burstein, Condon, and Yin 1987). The positive correlation found above supports the idea that a substantial part of the FUV flux of elliptical galaxies may be related to the activities in the nuclear region in a direct and/or an indirect way.

IV. DISCUSSION

With the results of the correlation studies in the preceding section in hand, in this section we discuss the star formation activity for spiral galaxies and explore the nature of the sources of the FUV radiation in elliptical galaxies.

a) Spiral Galaxies

In spiral galaxies, the total blue luminosity was supposed to be a good indicator of the recent star formation activity of middle to high mass stars (e.g., Trinchieri, Fabbiano, and Bandiera 1989). Sage and Solomon (1989), however, pointed out on the basis of studies of CO luminosity that the blue luminosity is not an accurate indicator because of the wide range of spectral types contributing to it. This trend was also suggested for infrared luminous galaxies by Devereux and Eales (1989) in the study of far-infrared luminosities and the nonthermal radio fluxes. Luminosities in much shorter wavelength regions should more directly indicate the ongoing star formation activity (Donas *et al.* 1987).

The FUV flux of spiral and irregular galaxies is supposed to be dominated by the radiations from hot luminous stars which have been born in the past few 10^7 yr. Under this condition the star formation rate (SFR) can be derived from FUV luminosity with the aid of simple galaxy evolution models (Lequeux *et al.* 1981; Donas *et al.* 1987).

Lequeux (1980) pointed out the importance of FUV observations in the study of the initial mass function (IMF) in galaxies. Donas and Deharveng (1984) analyzed the data obtained by *OAO 2* with careful corrections of the internal extinction, showing that the flux at 190 nm is in fact a good tracer of recent star formation. Donas *et al.* (1987) reported the balloon observations of total fluxes at 200 nm for a number of galaxies and confirmed that the star formation rate estimated from the total flux at 200 nm is in good agreement with those obtained from Hα observations (Kennicutt and Kent 1983; Kennicutt 1983*b*).

In order to estimate the star formation rate of the late-type galaxies in the Virgo Cluster, a simple galaxy model was calculated to be applied to the present data. The star formation rate (SFR), the initial mass function (IMF), and the other galaxy parameters were assumed to be constant in the past 10^8 yr. The model calculations were similar to those made by Lequeux *et al.* (1981) with minor revisions in the adopted evolution tracks and the estimation of FUV flux of early-type stars. The details

© American Astronomical Society • Provided by the NASA Astrophysics Data System

1990ApJ...363..422K

of the calculations are given in Appendix B together with some comments.

With the above models, SFR can be simply described as

$$\text{SFR}\ (M_\odot\ \text{yr}^{-1}) = \frac{L\ (\text{GUV})}{a \times 10^{39}\ \text{ergs s}^{-1}\ \text{Å}^{-1}}, \qquad (1)$$

where L is to be the FUV luminosity derived from the GUV observations. The value of the dimensionless constant a depending on the IMF is 3.4, when we take Lequeux's IMF (Lequeux 1980). The calculation shows that about one-half of the FUV flux comes from stars of masses between 5 and 10 $M_\odot$. Thus, the SFR derived from equation (1) indicates the SFR in middle-mass stars. When we adopt the FUV flux corrected for the intrinsic absorption in each galaxy, $f_{\lambda,c}$ (156 nm), and the Galactic extinction of 0.4 mag at 150 nm (Paper I), equation (1) with $a = 3.4$ is transformed into

$$\text{SFR}\ (M_\odot\ \text{yr}^{-1}) = \frac{f_{\lambda,c}\ (156\ \text{nm})}{3.6 \times 10^{-14}\ \text{ergs s}^{-1}\ \text{cm}^{-2}\ \text{Å}^{-1}}, \qquad (2)$$

for the distance of the Virgo Cluster of 21.9 Mpc.

The resulting SFR is in a range of $1 \sim 10\ M_\odot\ \text{yr}^{-1}$ for late-type galaxies in the central region of the Virgo Cluster, and SFRs for NGC 4501, NGC 4535, and NGC 4569 are compatible with those evaluated from Hα emission (Kennicutt 1983*a*, *b*) if the above-mentioned differences in the adopted models are taken into account.

When the corrected FUV flux is plotted against the H I 21 cm flux, a positive correlation with the slope of about unity is seen just as in Figure 4. The UV luminosity at 200 nm of galaxies was also shown to be linearly correlated with H I flux by Donas *et al.* (1987). If the FUV flux is simply proportional to SFR in the galaxy as indicated by equation (1) and the H I 21 cm flux correctly traces the content of atomic gas in galaxies, the linear relation may imply that SFR per unit volume is proportional to the gas density. The correlation, however, indicates the interrelation among the global parameters of galaxies and the local star formation rate could differ from this roughly linear relation.

In Figure 8 we compare SFR per unit blue luminosity (L_B) or per unit gas mass (M_g) between the Virgo galaxies and field galaxies. The data for the field galaxies were taken from Donas *et al.* (1987) who used the UV flux at 200 nm and slightly different stellar evolution models from the present ones. The effect of the differences on SFR is given in Appendix B, which hardly affects the general trends of Figure 8. The blue luminosity was estimated from B_T°, assuming the solar value $B_T^\circ = -26.09$. Only galaxies in Donas *et al.* (1987) which have B_T° listed in RC2 were used for field galaxies. For Virgo spirals, B_T's were taken from BST and B_T°'s were calculated according to RC2. The gas mass can be estimated from the H I 21 cm flux under the conditions of constant ratio M_g/M (H I) = 1.3 and of the optically thin configuration. The quantities SFR, L_B, and M_g have the same dependence on the distance; thus, their ratios are distance-independent parameters. We find practically no systematic difference in SFR per unit gas mass between the Virgo galaxies and field galaxies, but a clear difference in SFR per unit blue luminosity.

Figure 8 indirectly shows the established fact that the Virgo spirals in the central region are H I–deficient (Haynes, Giovanelli, and Chincarini 1984), and the remarkable finding that the SFR is reduced almost proportionally to the H I deficiency. This is also in agreement with the results of Hα observations

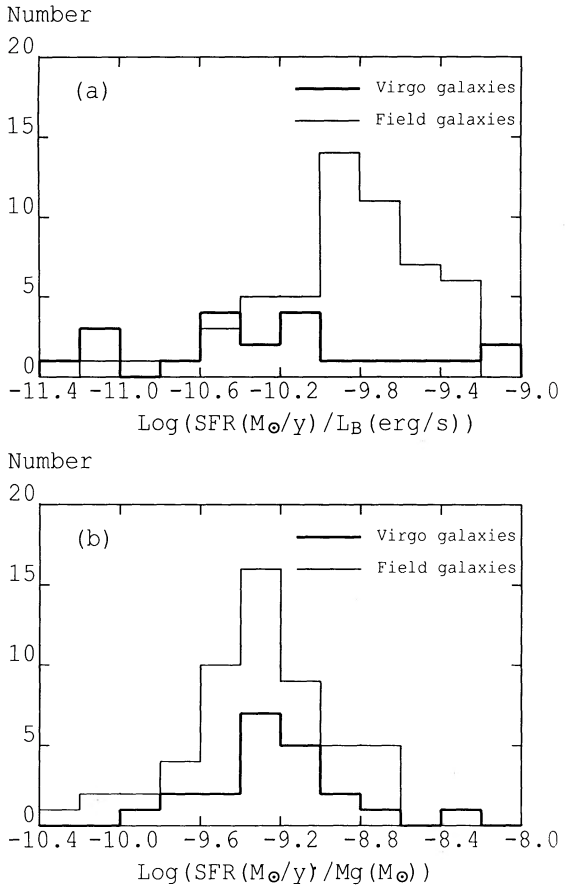

FIG. 8.—The histogram for the comparison of the star formation rate (SFR) (in $M_\odot\ \text{yr}^{-1}$) between the spiral galaxies in the field (*thin line*) and in the Virgo Cluster center (*thick line*). The abscissae are (*a*) the logarithm of SFR normalized by the blue luminosity (L_B) (in ergs s^{-1}) and (*b*) the logarithm of SFR normalized by the gas mass (M_g) (in $M_\odot$).

(Kennicutt 1983*a*) and the study of FIR observations (Doyon and Joseph 1989). Giovanelli and Haynes (1983, 1985) made it clear that the H I deficiency might be caused by stripping to decrease the radius of the gas distribution without substantially altering the average surface density of H I. According to them, the average H I deficiency factor of the galaxies within the circle of 5° radius in the Virgo Cluster center is 2.7, which is consistent with Figure 8. Since the present Virgo sample includes more spirals of $T \leq 5$ than those of $T > 5$, we have made a figure for galaxies only of $0 \leq T \leq 5$ both in the field and in the Virgo center. However, we have noticed no essential changes from Figure 8. On the other hand, the content of CO in the Virgo spirals seemed to be normal, and the observations confirmed the deficiency of H I relative to CO in the central region of the cluster (Kenney and Young 1986; Stark *et al.* 1986). No apparent depletion in FIR radiation is reported for the Virgo galaxies (Kenney and Young 1988), supporting the enhancement of FIR flux in Figure 5 relative to the H I 21 cm flux in Figure 4.

Based upon the above findings, we infer that the contents of the molecular clouds are normal in the spiral galaxies in the Virgo center relative to field spirals, but that the star formation activity and the content of H I gas are depleted in the former. This inference may further suggest that the interstellar molecules are concentrated in the inner part of spiral galaxies while

© American Astronomical Society • Provided by the NASA Astrophysics Data System

1990ApJ...363..422K

the H I gas, which may be a dominant indicator of the formation rate of middle-mass stars, is depleted due to the continuous stripping in the outer part of the Virgo galaxies. From Figure 8 we notice that the consumption time scale of gas by the star formation activity is as short as 10^9–4×10^9 yr, roughly the same as that of field galaxies investigated by Donas *et al.* (1987).

b) Elliptical Galaxies

For early-type galaxies, the interpretation of the FUV emission is still controversial. The interpretation of the turn-up may be divided into four categories based upon the following main components: young stars, hot HB stars, PAGB stars, and binary stars. The drawbacks and potential problems of each model are summarized in Bertelli, Chiosi, and Bertola (1989). De Boer (1985) discussed the FUV turn-up of ellipticals in connection with the blue population of globular clusters. Burstein *et al.* (1988) reported *IUE* observation of about 30 elliptical galaxies, indicating a correlation of the FUV turn up with the metallicity index Mg_2 (see also Faber 1983). Bertelli, Chiosi, and Bertola (1989) showed that the correlation can be explained by evolved stars using the latest models of evolutionary tracks if the helium abundance increases with metallicity. A similar conclusion was reached by Barbaro and Olivi (1989). However, they did not rule out the possibility that other sources are contributing to the FUV emission in elliptical galaxies. Bertola *et al.* (1986) and Bertola (1987) had pointed out that an additional contribution from continuing star formation inferred from the cooling flow might be superposed on the fundamental source given by PAGB stars and that the additional contribution might vary from galaxy to galaxy.

The elliptical galaxies we observed are bluer than $\log f_\lambda$ (156 nm) $- \log f_\lambda$ (550 nm) $\simeq -2$. Some of them were observed by Burstein *et al.* (1988), showing a color of m (156 nm) $- V < 3.5$ in the *IUE* aperture. According to Figure 1 in Burstein *et al.* (1988), we judge that the FUV turn-up of the observed galaxies may show a large scatter almost independently of the metallicity, and that the main cause of the color variation among them may have to be sought somewhere else. This further indicates that the FUV ellipticals we observed may have substantial additional FUV sources other than evolved stars. We will explore the possibility that the extra FUV sources are of a young population including young hot stars. Actually the observational results of Burstein *et al.* (1988) confirmed that early-type galaxies with noticeable ongoing star formation activity and "active" galaxies showed enhanced FUV radiation from the central region. Our observation also indicated that the dwarf elliptical with a prominent nucleus, IC 3457, might exhibit enhanced FUV radiation and behave like a spiral galaxy in the two-color diagram, Figure 3. We tentatively assume that even "normal" ellipticals may conceal additional extra FUV sources of young population in the central region of galaxies.

In this connection, the correlations of FUV flux with X-ray flux and radio flux we found in Figure 6 and 7 for FUV–bright galaxies of $T < 0$ suggest that the hot interstellar matter in these galaxies may finally fuel the nuclear radio activities, as pointed out by Fabbiano, Gioia, and Trinchieri (1989), and stimulate the star-forming activity in the central region. Walsh *et al.* (1989) suggested in their correlation study between FIR and radio flux of elliptical galaxies that the nuclear activity may be fueled by the interstellar matter emitting FIR.

In an attempt to estimate the contribution from the central region of ellipticals to the total FUV flux, we examine the ratio of the fluxes observed by *IUE* and GUV. The visual flux in a circular aperture with a diameter of 14″, which is supposed to represent the flux in the *IUE* aperture fairly well, was taken from Burstein *et al.* (1988). The fluxes at 156 nm and 242 nm in the *IUE* aperture were estimated by applying each filter on the *IUE* spectra by Burstein *et al.* (1988) (Paper I). The filter function of the observation by Smith and Cornett (1982) has a long-wavelength tail ($\lambda > 330$ nm), which was neglected in the present estimate. The error due to this neglect is estimated to be about 20% for NGC 4486 and NGC 4472 whose visual spectra in the *IUE* aperture are available. This does not affect the present conclusion. The total fluxes at 242 nm and in the V band were taken from Smith and Cornett (1982) and Watanabe (1983). The resulting ratios are summarized in Table 3 for five ellipticals for which the set of necessary data are available. The "central" to the total FUV flux varies from ~ 0.15 to > 0.4 among these galaxies.

We further assume that the basic extended components of FUV flux (f_B) are related to the old population such as evolved stars and behave proportionally to the visual flux; $f_B = \beta f_\lambda$ (550 nm). Since the aperture size of the *IUE* observation was fixed independent of the galaxy size, we assume that the extra FUV sources in the "central" region (f_A) are restricted within the *IUE* aperture area. It turns out that β ranges from 5×10^{-3} to 3×10^{-2} roughly corresponding to a range which could be induced by the variation of Mg_2 index from 0.30 to 0.35 (Burstein *et al.* 1988), and the ratio f_A/f_B from 0.5 for NGC 4374 to 0.13 for NGC 4472, as are given in Table 3. Although this ratio may serve to evaluate the FUV flux from the extra central sources of these elliptical galaxies, we need spatially resolved

TABLE 3

CENTRAL CONCENTRATION OF FUV FLUX IN GALAXIES

PARAMETER	GALAXY NAME				
	NGC 4374	NGC 4406	NGC 4472	NGC 4486	NGC 4552
IUE/Total Ratio[a]:					
156 nm	0.42	>0.43	0.16	0.16	0.34
242 nm	0.078	0.11	0.095	0.15	0.23
550 nm	0.111	0.071	0.050	0.04	0.15
f_A/f_B[b]	0.53	>0.63	0.13	0.14	0.29
$10^2 \times \beta$[c]	0.55	<0.29	1.07	2.72	2.71

[a] The ratio of the flux in the *IUE* aperture to the total flux.
[b] The ratio of the central component to the extended component (see text).
[c] The ratio of FUV to visual flux of the extended component multiplied by 100 (see text).

© American Astronomical Society • Provided by the NASA Astrophysics Data System

1990ApJ...363..422K

FUV images in order to clarify the problem further. *HST* images may contribute to solve this.

In a trial to interpret the FUV flux from the central region of ellipticals by star formation activity, we simply apply the same star formation model to elliptical galaxies as to spirals. Equation (2) gives the star formation rate of about $0.1 \sim 1\ M_\odot\ \mathrm{yr}^{-1}$ for the ellipticals whose FUV fluxes were detected in the present observations. This is roughly in agreement with the values of mass deposition rate estimated from X-ray observations based upon the cooling flow model (Thomas *et al.* 1986). Since part of the FUV fluxes may come from old populations (O'Connell and McNamara 1988) and since there is a large uncertainty in the estimation of mass deposition rate from X-ray data (Fabbiano 1989), this agreement might be coincidental. However, if the additional sources of FUV to PAGB stars in ellipticals are in fact recently born stars caused by the cooling flow, it may be noteworthy that the birthrate derived from the FUV flux with the standard IMF is, in a sense of the order of magnitude estimate, consistent to the prediction from the cooling flow model. It should be added, however, that since some elliptical galaxies in the present sample indicate the depletion of the 242 nm flux relative to the 156 nm flux compared to the spirals (see Fig. 3), their IMF may be enhanced rather in massive stars differently from that for spiral galaxies.

Finally we wish to point out the anomalous behaviors of the pair of giant ellipticals, NGC 4406 (M86) and NGC 4374 (M84), in Figures 6 and 7. In particular, the drastic inversion of the ratio of the X-ray to the radio flux between the two galaxies is noticeable, together with the high concentration ($f_A/f_B > 0.63$) and the low total flux of FUV of NGC 4406 relative to NGC 4374. These anomalies might be related to the special situation of the pairs of giant ellipticals in the Virgo Cluster. NGC 4406 is known to be radio-faint, but to have a large asymmetric X-ray halo, suggesting the drastic interaction between the interstellar matter and the intercluster medium (Forman *et al.* 1979; Fabian, Schwarz, and Forman 1980). This kind of interaction may strongly affect the star formation activity and/or the nuclear activity of the interacting galaxies, but it is not expected to affect the evolution and/or the extended distribution of aged stars, consequently not the FUV flux from evolved stars. This line of consideration indicates that the dominant part of FUV flux of some elliptical galaxies may still originate from young population around the central region substantially larger than the *IUE* aperture size.

The authors wish to acknowledge their thanks to K. S. de Boer for his helpful comments, to Mrs. T. Masuyama for preparing the manuscript, and to the experiment team of the GUV rocket observation for their cooperation. This study was partly supported by grant-in-aid 59065002 from the Ministry of Education, Science, and Culture.

APPENDIX A

ANONYMOUS OBJECTS

Table 4 shows positions of the objects detected by GUV which have not been listed in previous catalogs. The object designation is given in column (1), GUV position in column (2), FUV flux f_λ (156 nm) and its error in units of 10^{-14} ergs cm^{-2} s^{-1} Å^{-1} in column (3), and the previous designation in Paper I, if any, in column (4). Possible candidate sources were examined on the Palomar Sky Survey Print (PSSP). Except for the sources reported in Paper I, the individual anonymous sources will be commented on below.

A1221+09.7.—SAO 119374 is located close to this GUV position. The star is a K0 star of $m_V = 8.9$.

A1221+12.7.—There are faint stellar objects around this source position, but their colors are uncertain in PSSP.

A1224+14.2.—SAO 100100 is close to this source position. The star is a K0 star of $m_V = 8.4$.

A1224+08.8.—There are faint stellar objects without color information.

A1230+13.2.—There is a bluish faint star on this position.

A1231+14.5.—This is located in the north edge of the GUV1 picture, and its flux and position may be subject to large uncertainties. There is a bluish faint star on this position.

A1231+10.7.—There is a stellar object, but its color is not certain.

TABLE 4

ANONYMOUS OBJECTS

Name (1)	Position (1950) α, δ (2)	f_λ (156 nm) (10^{-14} ergs cm^{-2} s^{-1} Å^{-1}) (3)	Notes (4)
A1221+09.7.....	12^{h}21^m.7, 09°48′	1.93 ± 0.46	
A1221+12.7.....	12 21.8, 12 42	0.90 ± 0.48	
A1224+14.2.....	12 24.4, 14 14	2.86 ± 0.54	
A1224+08.8.....	12 24.6, 08 49	1.45 ± 0.36	
A1225+11.5.....	12 25.0, 11 31	4.46 ± 0.64	P2
A1225+11.8.....	12 25.3, 11 54	8.16 ± 0.51	P3
A1227+08.6.....	12 27.0, 08 39	3.42 ± 0.47	P7
A1230+13.2.....	12 30.5, 13 15	0.95 ± 0.35	
A1231+14.5.....	12 31.2, 14 31	2.60: ± 0.46	
A1231+10.7.....	12 31.3, 10 42	1.02 ± 0.36	
A1232+09.7.....	12 32.6, 09 44	9.82 ± 0.59	P17
A1234+09.9.....	12 34.8, 09 56	0.86 ± 0.31	
A1235+10.2.....	12 35.5, 10 17	2.77 ± 0.42	P22

© American Astronomical Society • Provided by the NASA Astrophysics Data System

1990ApJ...363..422K

A1234+09.9.— NGC 4578 is close to this object, but the difference in position is significant. The detection level is not very high, and there is a possibility that the detected flux enhancement was spurious.

A1235+10.2.—This is the object reported as P22 in Paper I without definite candidates. This is located on the edge of the GUV2 picture. The revised flux turned out to be about one-half of that reported in Paper I, owing to the correct estimate of the background increasing toward the edge of the picture.

APPENDIX B

ESTIMATE OF STAR FORMATION RATE

We adopt models of 100, 80, 60, 50, 40, 30, and 20 $M_\odot$ by de Loore, de Grève, and Vanbeveren (1978) with $N = 300$ (mass-loss parameter); that of 15 $M_\odot$ by Maeder (1981) of case C; those of 11, 9, and 7 $M_\odot$ by Becker (1981) ($Y = 0.38$ and $Z = 0.03$); those of 5, 3, and 2 $M_\odot$ by Alcock and Pazyński (1978) ($X = 0.7$ and $Z = 0.03$); and 1.75, 1.40, 1.25, 1.10, 1.00, and 0.90 $M_\odot$ models by Mengel *et al.* (1979) with $Y = 0.30$ and $Z = 0.04$.

We took the UV photometric results of early-type stars by *ANS* (Wesselius *et al.* 1980) to obtain FUV colors of the stars. For stars with $T_{\rm eff} \geq 40{,}000$ K, we extrapolated the *ANS* color rather than to take the model calculations by Kurucz (1979) since the differences between models and observations for such high-temperature stars are not negligible (Wesselius *et al.* 1980). The contribution from very high mass stars is not large and thus the results are not sensitive to this choice.

For bolometric corrections, the results by Code *et al.* (1976) were adopted. Since the absolute scale of GUV was found to be about 80% of *TD 1* (Paper I) and the scale of *ANS* to *TD 1* was about 90% (Koornneef *et al.* 1982), the ratio of the absolute scale of GUV to *ANS* was estimated to be 86%.

The value of the constant a in equation (1) is 3.4 for Lequeux's IMF (Lequeux 1980). When we use the FUV luminosity at 200 nm in place of L (GUV), the constant a becomes 2.8 for the present model with the Lequeux's IMF. This value is somewhat smaller (about 30%) compared to the value for the model adopted by Donas *et al.* (1987); most difference was confirmed to originate from that in adopted stellar models. For a Miller-Scalo IMF (Miller and Scalo 1979) $a = 1.5$, while $a = 6.8$ is obtained for IMF $\propto M^{-2.5}$ at the high-mass end (Kennicutt 1983*b*). Thus the uncertainty of a due to different IMFs is a factor of 3–5. However, the ratio of the values of a at FUV (150 nm) and at 200 nm was found to be between 1.4 and 1.6, being relatively insensitive to the choice of IMF. Thus, the comparative discussion in § IV using SFRs derived from 200 nm photometry and GUV observation is hardly affected by the choice of IMF.

REFERENCES

Alcock, C., and Pazyński, B. 1978, *Ap. J.*, **223**, 244.
Barbaro, G., and Olivi, F. M. 1989, *Ap. J.*, **337**, 125.
Becker, S. A. 1981, *Ap. J. Suppl.*, **45**, 475.
Bender, R., Surma, P., Döbereiner, S., Möllenhoft, C., and Madejsky, R. 1989, *Astr. Ap.*, **217**, 35.
Bertelli, G., Chiosi, C., and Bertola, F. 1989, *Ap. J.*, **339**, 889.
Bertola, F. 1987, in *Proc. NATO Advanced Research Workshop, Cooling Flows in Clusters and Galaxies*, ed. A. C. Fabian (Dordrecht: Kluwer), p. 127.
Bertola, F., Cappaccioli, M., Holm, A. V., and Oke, J. B. 1980, *Ap. J. (Letters)*, **237**, L65.
Bertola, F., Cappaccioli, M., and Oke, J. B. 1982, *Ap. J.*, **254**, 494.
Bertola, F., Gregg, M. D., Gunn, J. E., and Oemler, A. 1986, *Ap. J.*, **303**, 624.
Binggeli, B., Sandage, A., and Tammann, G. A. 1985, *A.J.*, **90**, 1681 (BST).
Bohlin, R. C., Cornett, R. H., Hill, J. K., Hill, R. S., O'Connell, R. W., and Stecher, T. P. 1985, *Ap. J. (Letters)*, **298**, L37.
Bohlin, R. C., Cornett, R. H., Hill, J. K., Hill, R. S., and Stecher, T. P. 1988, *Ap. J.*, **334**, 657.
Bohlin, R. C., Cornett, R. H., Hill, J. K., Smith, A. M., and Stecher, T. P. 1983, *Ap. J. (Letters)*, **274**, L53.
Bohlin, R. C., Hill, J. K., Stecher, T. P., and Witt, A. N. 1982, *Ap. J.*, **255**, 87.
Burstein, D., Bertola, F., Buson, L. M., Faber, S. M., and Lauer, T. R. 1988, *Ap. J.*, **328**, 440.
Burstein, D., Condon, J. J., and Yin, Q. F. 1987, *Ap. J. (Letters)*, **315**, L99.
Canizares, C., Fabbiano, G., and Trinchieri, G. 1987, *Ap. J.*, **312**, 503.
Carnochan, D. F., Navach, C., and Wilson, R. 1975, *M.N.R.A.S.*, **172**, 27P.
Carruthers, G. R., Heckathorn, H. M., and Opal, C. B. 1978, *Ap. J.*, **225**, 346.
Carruthers, G. R., and Opal, C. B. 1977*a*, *Ap. J. (Letters)*, **212**, L27.
———. 1977*b*, *Ap. J.*, **217**, 95.
Code, A. D., and Welch, G. A. 1979, *Ap. J.*, **228**, 95.
———. 1982, *Ap. J.*, **256**, 1.
Code, A. D., Davis, J., Bless, R. C., and Hanbury-Brown, R. 1976, *Ap. J.*, **203**, 417.
Condon, J. J. 1987, *Ap. J. Suppl.*, **65**, 485.
Condon, J. J., Yin, Q. F., and Burstein, D. 1987, *Ap. J. Suppl.*, **65**, 543.
de Boer, K. S. 1982, *Astr. Ap. Suppl.*, **50**, 247.
———. 1985, *Astr. Ap.*, **142**, 321.
Deharveng, J. M., Jakobsen, P., Milliard, B., and Laget, M. 1980, *Astr. Ap.*, **88**, 52.
de Loore, C., de Grève, J. P., and Vanbeveren, D. 1987, *Astr. Ap. Suppl.*, **34**, 363.
de Vaucouleurs, G., de Vaucouleurs, A., and Corwin, H. G., Jr. 1976, *Second Reference Catalogue of Bright Galaxies* (Austin: University of Texas Press) (RC2).
Devereux, N. A., and Eales, S. A. 1989, *Ap. J.*, **340**, 708.
Donas, J., and Dharveng, J. M. 1984, *Astr. Ap.*, **140**, 325.
Donas, J., Deharveng, J. M., Laget, M., Milliard, B., and Huguenun, D. 1987, *Astr. Ap.*, **180**, 12.
Donas, J., Milliard, B., Laget, M., and Deharveng, J. M. 1981, *Astr. Ap.*, **97**, L7.
Doyon, R., and Joseph, R. D. 1989, *M.N.R.A.S.*, **239**, 347.
Fabbiano, G. 1989, *Ann. Rev. Astr. Ap.*, **27**, 87.
Fabbiano, G., Gioia, I., and Trinchieri, G. 1989, *Ap. J.*, **347**, 127.
Fabbiano, G., and Trinchieri, G. 1985, *Ap. J.*, **296**, 430.
Fabbiano, G., Trinchieri, G., and Macdonald, A. 1984, *Ap. J.*, **284**, 65.
Faber, S. M. 1983, *Highlights Astr.*, **6**, 165.
Fabian, A. C., Schwarz, J., and Forman, W. 1980, *M.N.R.A.S.*, **192**, 135.
Forman, W., Jones, C., and Tucker, W. 1985, *Ap. J.*, **293**, 102.
Forman, W., Schwarz, J., Jones, C., Liller, W., and Fabian, A. 1979, *Ap. J. (Letters)*, **234**, L27.
Giovanelli, R., and Haynes, M. P. 1983, *A.J.*, **88**, 881.
———. 1985, *Ap. J.*, **292**, 404.
Haynes, M. P., Giovanelli, R., and Chincarini, G. L. 1984, *Ann. Rev. Astr. Ap.*, **22**, 445.
Helou, G., Giovardi, C., Salpeter, E. E., and Krumm, N. 1981, *Ap. J. Suppl.*, **46**, 267.
Helou, G., Huffman, G. L., and Salpeter, E. E. 1984, *Ap. J. Suppl.*, **55**, 433.
Helou, G., Khan, I. R., Malek, L., and Boehmer, L. 1988, *Ap. J. Suppl.*, **68**, 151.
Hill, J. K., Bohlin, R. C., and Stecher, T. P. 1984, *Ap. J.*, **277**, 542.
Huchtmeier, W. K., and Richter, O.-G. 1986, *Astr. Ap. Suppl.*, **64**, 111.
Huffman, G. L., Helou, G., Salpeter, E. E., Glosson, J., and Sandage, A. 1987, *Ap. J. Suppl.*, **63**, 247.
Huffman, G. L., Lewis, B. M., Helou, G., Salpeter, E. E., and Williams, H. L. 1989, *Ap. J. Suppl.*, **69**, 65.
Jura, M., Kim, D. W., Knapp, G. R., and Guhathakurta, P. 1987, *Ap. J. (Letters)*, **312**, L11.
Kennicutt, R. C., Jr. 1983*a*, *A.J.*, **88**, 483.
———. 1983*b*, *Ap. J.*, **272**, 54.

© American Astronomical Society • Provided by the NASA Astrophysics Data System

1990ApJ...363..422K

Kennicutt, R. C., Jr., and Kent, S. M. 1983, *A.J.*, **88**, 1094.
Kenney, J. D., and Young, J. 1986, *Ap. J.* (*Letters*), **301**, L13.
———. 1988, *Ap. J.*, **326**, 588.
Knapp, G. R., Guhathakurta, P., Kim, D.-W., and Jura, M. 1989, *Ap. J. Suppl.*, **70**, 329.
Koornneef, J., Meade, M. R., Wesselius, P. R., Code, A. D., and van Duinen, R. J. 1982, *Astr. Ap. Suppl.*, **47**, 341.
Kurucz, R. L. 1979, *Ap. J. Suppl.*, **40**, 1.
Lequeux, J. 1980, in *Star Formation, 10th Advanced Course of the Swiss Society of Astronomy and Astrophysics*, ed. A. Maeder and L. Martinet (Saas-Feé: Geneva Observatory), p. 75.
Lequeux, J., Maucherat-Joubert, M., Deharveng, J. M., and Kunth, D. 1981, *Astr. Ap.*, **103**, 305.
Maeder, A. 1981, *Astr. Ap.*, **102**, 401.
Mengel, J. G., Sweigart, A. V., Denarque, P., and Gross, P. G. 1979, *Ap. J. Suppl.*, **40**, 733.
Miller, G. E., and Scalo, J. M. 1979, *Ap. J. Suppl.*, **41**, 513.
Nilson, P. 1973, *Uppsala General Catalogue of Galaxies* (Uppsala: Acta Universitatas).
O'Connell, R. W., and McNamara, B. R. 1987, in *Proc. NATO Advanced Research Workshop, Cooling Flows in Clusters and Galaxies*, ed. A. C. Fabian (Dordrecht: Kluwer), p. 103.
Onaka, T., *et al.* 1989, *Ap. J.*, **342**, 238 (Paper I).
Sage, L. J., and Solomon, P. M. 1989, *Ap. J.* (*Letters*), **342**, L15.
Smith, A. M., and Cornett, R. H. 1982, *Ap. J.*, **261**, 1.
Stark, A. A., Knapp, G. R., Bally, J., Wilson, R. W., Penzias, A. A., and Rowe, E. 1986, *Ap. J.*, **310**, 660.
Stecher, T. P., Bohlin, R. C., Hill, J. K., and Jura, M. A. 1982, *Ap. J.* (*Letters*), **255**, L99.
Thomas, P. A., Fabian, A. C., Arnaud, K. A., Forman, W., and Jones, C. 1986, *M.N.R.A.S.*, **222**, 655.
Trinchieri, G., Fabbiano, G., and Bandiera, R. 1989, *Ap. J.*, **342**, 759.
Walsh, D. E. P., Knapp, G. R., Wrobel, J. M., and Kim, D.-W. 1989, *Ap. J.*, **337**, 209.
Watanabe, M. 1983, *Ann. Tokyo Astr. Obs.*, 2d Ser., **19**, 121.
Wesselius, P. R., van Duinen, R. J., Aalders, J. W. G., and Kester, D. 1980, *Astr. Ap.*, **85**, 221.
Wesselius, P. R., van Duinen, R. J., de Jonge, A. R. W., Aalders, J. W. G., Luinge, W., and Wildeman, K. J. 1982, *Astr. Ap. Suppl.*, **49**, 427.

K. KODAIRA and T. WATANABE: National Astronomical Observatory, Japan, Mitaka, Tokyo 181, Japan

T. ONAKA and W. TANAKA: Department of Astronomy, Faculty of Science, University of Tokyo, Tokyo 113, Japan

© American Astronomical Society • Provided by the NASA Astrophysics Data System